Double formates $Ba_2M(HCOO)_6(H_2O)_4$ (M = Co, Ni, Cu, Zn): crystal structures and hydrogen bonding systems

R. Baggio[a], D. Stoilova[b,*], G. Polla[a], G. Leyva[a], M.T. Garland[c]

[a]*Depto. de Física, Comisión Nacional de Energía Atómica, Av. Gral Paz 1499, 1650 San Martín, Pcia. de Buenos Aires, Argentina*
[b]*Institute of General and Inorganic Chemistry, Acad. G. Bonchev Street, Building 11, Bulgarian Academy of Sciences, 1113 Sofia, Bulgaria*
[c]*Depto de Física, Fac. de Ciencias Físicas y Matemáticas, U. de Chile, Av. Blanco Encalada 2008, Santiago de Chile, Chile*

Abstract

The crystal structures of four members in the isomorphous series, $Ba_2M(HCOO)_6(H_2O)_4$ (M = Co, Ni, Cu, Zn) are presented and thoroughly discussed. Discrepancies with a previous structural report on the Cu isolog [Z. Kristallogr. 110 (1958) 231] were cleared out through a re-refinement of the original data, the outcome of which definitely confirmed the present results. The strengths of the hydrogen bonds in the title compounds as deduced from the infrared wavenumbers of the uncoupled OD stretches of matrix-isolated HDO molecules are discussed in terms of the $O_w\cdots O$ hydrogen bond lengths, the different hydrogen bond acceptor capabilities of the formate oxygen atoms and the weak $Ba-OH_2$ interactions. The proton acceptor strength of the oxygen atoms is evaluated within the framework of the Brown's bond-valence theory. The intramolecular OH bond lengths are derived from the novel ν_{OD} vs. r_{OH} correlation curve [J. Mol. Struct. 404 (1997) 63].

Keywords: Double formates $Ba_2M(HCOO)_6(H_2O)_4$ (M = Co, Ni, Cu, Zn); Crystal structures; Matrix IR spectroscopy; Hydrogen bond strength

1. Introduction

The title compounds form isomorphous crystals with close unit-cell parameters [1,2]. Of these, the only structure so far reported in the literature was that of the copper analogue [2], where the copper ions were described as being octahedrally surrounded by six oxygen atoms, four coming from formate groups and the rest being water molecules. In previous papers of one of the authors, the hydrogen bond strengths, the water librations and the vibrational behavior of the $HCOO^-$ ions in the double formates have been analyzed by means of infrared spectroscopy (ambient temperature) [1,3]. The IR spectra in the region of ν_{OD} of matrix-isolated HDO molecules (isotopically dilute samples) reveals that hydrogen bonds of almost equal strength are formed in the four compounds. However, these spectroscopic findings could not be explained if water molecules are assumed to coordinate M^{2+} ions (Cu, Co, Ni, Zn), since these ions are known to display different $M-OH_2$ interactions (synergetic effect) due to the different degree of covalency of the respective bonds [4–8].

This fact prompted us to study the structures of $Ba_2M(HCOO)_6(H_2O)_4$ (M = Co, Ni, Zn) by single crystal X-ray measurements. Since the results reported in Rao's work [2] are characterized by the low precision attainable at the time, which did not allow the authors to make a meaningful H-bonding description of the system, the crystal structure of the copper compound was re-investigated as well. IR spectra in the region of the O–H and O–D stretches recorded at liquid nitrogen temperature are also presented and discussed with respect to the corresponding hydrogen bond lengths and the crystal structure properties.

2. Experimental

The simple metal formates, $Ba(HCOO)_2$, $M(HCOO)_2(H_2O)_2$ (M = Co, Ni, Zn) and $Cu(HCOO)_2(H_2O)_4$, were prepared by neutralization of barium carbonate and the corresponding metal hydroxide carbonates with dilute

* Corresponding author. Tel.: +359-2-979-35-66; fax: +359-2-870-50-24.
E-mail address: stoilova@svr.igic.bas.bg (D. Stoilova).

formic acid solutions at 60–70 °C. Then the solutions were filtered, concentrated and cooled to room temperature. The crystals were filtered and dried in air. The double formates were prepared according to the solubilities in the three component systems $Ba(HCOO)_2$–$Cu(HCOO)_2$–H_2O at 25 °C [9] using the method of isothermal decrease of supersaturation (the other formates were prepared analogically). The isotopically dilute samples (matrix-isolated HDO molecules) were prepared by the same crystallization procedure in the presence of about 10% D_2O. The crystals obtained were filtered, washed with alcohol and dried in air. Single crystals were obtained by slow isothermal evaporation (at ambient temperature) of mixed supersaturated solutions from the crystallization field of the double salts. All reagents used were 'p.a.' (Merck).

Single crystal diffraction data were collected with monochromatic Mo Kα radiation, $\lambda = 0.71069$ Å on a Bruker AXS SMART APEX CCD diffractometer, using as software SMART [10] for data collection, SAINT [11] for integration and SADABS [12] for absorption corrections, all of them programs in the diffractometer package. The structures were solved by direct methods and difference Fourier, and refined by least squares on F^2 with anisotropic displacement parameters for non-H atoms. Hydrogen atoms in the formate groups were placed at their calculated positions and allowed to ride onto their host carbons both in coordinates as well as in thermal parameters. Those corresponding to water molecules were found in the final difference Fourier maps, and refined with a restrained O–H: 0.85(2)Å distance. For the H-bonding description these positions were corrected by sliding the hydrogen atoms along the corresponding O_w–H vectors so as to have O_w–H distances matching those provided by spectroscopic data. All calculations to solve the structures, refine the models proposed and obtain derived results were carried out with the computer programs SHELXS97 and SHELXL97 [13] and SHELXTL [14]. Full use of the CCDC package was also made for searching in the CSD Database [15]. A survey of crystallographic and refinement data, as well as fractional atomic coordinates and equivalent isotropic displacement factors are presented for all four compounds in Tables 1 and 2, while Table 3 shows relevant interatomic distances and angles and Table 4, H-bonding interactions.

Crystallographic data (excluding structure factors) have been deposited with the Cambridge Crystallographic Data Centre as supplementary publications no. CCDC 230288-230291. Copies of the data can be obtained free of charge on application to CCDC, 12 Union Road, Cambridge CB2 1EZ, UK (fax: +(44)-1223-336-033; e-mail: deposit@ccdc.cam.ac.uk).

The infrared spectra were recorded on a Bruker model IFS 113 Fourier transform interferometer (resolution <2 cm^{-1}) at ambient and liquid nitrogen temperatures. KBr discs were used as matrices. Ion exchange or other reactions with KBr have not been observed.

Table 1
Crystal data and structure refinement details for $Ba_2M(CHOO)_6(H_2O)_4$, (M = Co, Ni, Cu, Zn)

	M = Co (1)	M = Ni (2)	M = Cu (3)	M = Zn (4)
Empirical formula	$C_6\ H_{14}\ Ba_2\ Co\ O_{16}$	$C_6\ H_{14}\ Ba_2\ Ni\ O_{16}$	$C_6\ H_{14}\ Ba_2\ Cu\ O_{16}$	$C_6\ H_{14}\ Ba_2\ O_{16}\ Zn$
Formula weight	675.78	675.56	680.39	682.22
a (Å)	8.9191(7)	8.8809(7)	8.8166(9)	8.9357(8)
b (Å)	7.1394(6)	7.1281(5)	7.1279(7)	7.1394(6)
c (Å)	6.9062(6)	6.8970(5)	6.9281(7)	6.9018(6)
α (°)	99.4770(10)	99.3400(10)	98.000(2)	99.4100(10)
β (°)	108.8490(10)	108.8650(10)	108.9400(10)	108.7820(10)
γ (°)	82.4050(10)	82.4450(10)	82.546(2)	82.4530(10)
V (Å^3)	409.03(6)	406.21(5)	406.14(7)	409.79(6)
D_{calc} (g cm^{-3})	2.743	2.762	2.782	2.765
μ (mm^{-1})	5.845	6.023	6.175	6.286
$F(000)$	317	318	319	320
Crystal shape, color	Prisms, pale rose	Plates, light green	Plates, light blue	Prisms, colorless
θ range (°)	2.42–27.72	2.43–27.94	2.45–27.75	2.42–28.05
Index ranges	$-11 <= h <= 11$, $-8 <= k <= 9$, $-8 <= l <= 9$	$-11 <= h <= 11$, $-9 <= k <= 9$, $-8 <= l <= 8$	$-11 <= h <= 11$, $-9 <= k <= 9$, $-8 <= l <= 9$	$-11 <= h <= 11$, $-9 <= k <= 9$, $-9 <= l <= 8$
N_{tot}, $N_{uniq}(R_{int})$, $N_{[I>2\sigma(I)]}$	3411, 1749(0.012), 1688	3389, 1740(0.011), 1710	3346, 1717(0.0182), 1676	3423, 1769(0.0186), 1707
Goodness-of-fit S	0.931	0.987	1.071	0.932
R indices [$I > 2\sigma(I)$]	$R1 = 0.0180$, $wR2 = 0.0497$	$R1 = 0.0179$, $wR2 = 0.0506$	$R1 = 0.0223$, $wR2 = 0.0570$	$R1 = 0.0201$, $wR2 = 0.0525$
R indices (all data)	$R1 = 0.0190$, $wR2 = 0.0504$	$R1 = 0.0183$, $wR2 = 0.0509$	$R1 = 0.0239$, $wR2 = 0.0595$	$R1 = 0.0211$, $wR2 = 0.0534$
ρ_{max}/ρ_{min} (eÅ^{-3})	0.409 and −0.891	0.425 and −0.890	0.977 and −1.165	0.919 and −0.821

Details in common: T (K): 293(2), λ (Å): 0.71073, crystal system: triclinic, space group: $P-1$, Z: 1, parameters refined: 268, absorption correction: Multi_scan.

Table 2
Fractional atomic coordinates ($\times 10^4$) and equivalente isotropic temperature factors (e $Å^3 \times 10^3$)

Cpnd		x	y	z	U_{eq}	Cpnd		x	y	z	U_{eq}
M: Co (1)	Ba	−3516(1)	2662(1)	930(1)	14(1)	M: Ni (2)	Ba	−3511(1)	2658(1)	929(1)	15(1)
	Co	0	0	0	14(1)		Ni	0	0	0	15(1)
	C(1A)	1638(3)	−2041(4)	3530(4)	20(1)		C(1A)	1614(3)	−2022(4)	3514(4)	20(1)
	O(1A)	1635(2)	−1935(3)	1711(3)	20(1)		O(1A)	1621(2)	−1895(3)	1718(3)	20(1)
	O(2A)	2576(3)	−3077(3)	4729(3)	30(1)		O(2A)	2548(3)	−3069(3)	4718(3)	31(1)
	C(1B)	−8004(3)	2726(4)	−535(5)	21(1)		C(1B)	−8022(3)	2731(4)	−519(5)	20(1)
	O(1B)	−6884(3)	3474(3)	−682(3)	25(1)		O(1B)	−6900(2)	3472(3)	−702(4)	25(1)
	O(2B)	−8142(2)	967(3)	−729(3)	20(1)		O(2B)	−8160(2)	967(3)	−699(3)	20(1)
	C(1C)	1251(4)	2684(4)	3975(4)	24(1)		C(1C)	1258(3)	2659(4)	3950(4)	24(1)
	O(1C)	51(3)	2174(3)	2516(3)	24(1)		O(1C)	53(2)	2129(3)	2468(3)	23(1)
	O(2C)	2656(3)	2018(3)	4265(3)	31(1)		O(2C)	2666(2)	2014(3)	4259(3)	30(1)
	O(1W)	−5034(3)	172(3)	2402(3)	23(1)		O(1W)	−5029(2)	163(3)	2406(3)	24(1)
	O(2W)	−5023(3)	5786(3)	2910(3)	21(1)		O(2W)	−5033(2)	5778(3)	2907(3)	21(1)
M: Cu (3)	Ba	−3495(1)	2653(1)	977(1)	16(1)	M: Zn (4)	Ba	−3526(1)	2664(1)	931(1)	15(1)
	Cu	0	0	0	17(1)		Zn	0	0	0	16(1)
	C(1A)	1635(4)	−1910(5)	3496(5)	21(1)		C(1A)	1643(4)	−2034(5)	3521(5)	20(1)
	O(1A)	1600(3)	−1816(3)	1670(3)	21(1)		O(1A)	1644(2)	−1927(3)	1714(3)	20(1)
	O(2A)	2602(3)	−2958(4)	4692(4)	30(1)		O(2A)	2580(3)	−3063(4)	4729(3)	30(1)
	C(1B)	−8052(4)	2734(5)	−480(5)	21(1)		C(1B)	−8003(4)	2730(4)	−541(5)	20(1)
	O(1B)	−6915(3)	3468(4)	−624(4)	27(1)		O(1B)	−6881(3)	3479(3)	−678(4)	25(1)
	O(2B)	−8203(3)	959(3)	−685(3)	22(1)		O(2B)	−8137(2)	965(3)	−734(3)	20(1)
	C(1C)	1268(4)	2804(5)	4095(5)	26(1)		C(1C)	1262(4)	2684(5)	3974(5)	24(1)
	O(1C)	25(3)	2367(4)	2691(4)	29(1)		O(1C)	50(3)	2177(3)	2517(3)	24(1)
	O(2C)	2676(3)	2078(4)	4344(4)	31(1)		O(2C)	2656(3)	2020(4)	4260(3)	30(1)
	O(1W)	−5053(3)	129(4)	2388(4)	24(1)		O(1W)	−5037(3)	173(3)	2401(3)	23(1)
	O(2W)	−5013(3)	5762(3)	2861(3)	22(1)		O(2W)	−5022(3)	5787(3)	2912(3)	21(1)

The thermal experiments were carried out with simultaneous measurements of thermogravimetry and differential thermal analysis in a DTG-50/50 H Shimadzu apparatus, between 30 and 1000 °C, in static air, at a heating rate of 10 °C/min. Each sample was pulverized in an agatha mortar in order to carry out the thermal treatments under the same conditions for all four compounds. The decomposition products were identified by X-ray diffraction at ambient temperature, on a Philips PW-3710 diffractometer (Cu K_α radiation, $\lambda = 1.5418$ Å).

3. Results and discussion

3.1. Crystal structures

The compounds crystallize in the triclinic space group $P-1$, with an entire formula ($Ba_2M(CHOO)_6(H_2O)_4$, M = Co, Ni, Cu, Zn) per cell, only half of it being independent. As a consequence, the cation M must lay on a symmetry center (multiplicity 0.5) and the barium atom, in a general position (multiplicity 1).

Fig. 1 shows a molecular diagram of the assembly, as represented by the Co isolog. The barium atom is 10-fold coordinated to six carboxylate oxygens and four aqua molecules. The coordination polyhedron could be depicted as a severely distorted bi-capped square antiprism with one of its bases defined by all four aqua molecules (O1w, O1w#2, O2w and O2w#4; for symmetry codes refer to Table 1 footnote), the other one by O1A#1, O2B#2, O2A#3, O1B#4 and the carboxylate oxygens O1B and O1C occupying the capping positions.

The M octahedral site, while keeping the same coordination pattern throughout the whole series, offers the largest geometrical variants due to individual cation differences. This is clearly seen from the values presented in Table 3; thus, the Co and Zn moieties appear as almost identical in their distortions, the Ni one is almost isometrical and the Cu environment shows the largest departures from ideal values due to its usual Jahn Teller's distortion.

Inspection of Fig. 1 and Table 3 shows that the M environment is solely conformed by carboxylate oxygens. This fact is in conflict with the results reported in Ref. [2], where two symmetry related water molecules were ascribed to the copper coordination polyhedra. The absolute coincidence in composition, cell parameters, space group, cation's positions, etc. suggested they were the same compound, but in order to be sure we refined both models, Rao's and our's, using the ($hk0$) and ($h0l$) projection data included in the original work and under the same conditions. The results confirmed our model to be correct also for Rao's structure, with R indices of (0.151/0.126) and residual electron density peaks of (1.29, −1.25/0.99, −0.093 e $Å^3$), in a (Rao's/our's) sequence.

The high connectivity of the structure is achieved through the profuse involvement in coordination of

Table 3
Bond lengths (Å) and angles (°)

Bond/angle	M = Co (1)	M = Ni (2)	M = Cu (3)	M = Zn (4)
Ba–O(1A)#1	2.8008(19)	2.8046(18)	2.817(2)	2.797(2)
Ba–O(2B)#2	2.8143(19)	2.8130(18)	2.822(2)	2.811(2)
Ba–O(2W)	2.836(2)	2.838(2)	2.822(2)	2.828(2)
Ba–O(2A)#3	2.815(2)	2.820(2)	2.829(2)	2.812(2)
Ba–O(1W)	2.855(2)	2.850(2)	2.842(2)	2.842(2)
Ba–O(1B)	2.862(2)	2.868(2)	2.865(3)	2.840(2)
Ba–O(2W)#4	2.883(2)	2.878(2)	2.873(2)	2.876(2)
Ba–O(1B)#4	2.867(2)	2.865(2)	2.888(3)	2.859(2)
Ba–O(1W)#2	2.880(2)	2.876(2)	2.905(2)	2.877(2)
Ba–O(1C)	3.004(2)	2.988(2)	2.932(3)	2.999(2)
Ba–M	3.6310(3)	3.6143(2)	3.6078(3)	3.6283(3)
Ba–Ba#4	4.0840(4)	4.0823(3)	4.0855(4)	4.0634(4)
M–O(1A)	2.0790(18)	2.0506(17)	1.972(2)	2.073(2)
M–O(2B)#2	2.1052(19)	2.0713(18)	2.016(2)	2.103(2)
M–O(1C)	2.124(2)	2.081(2)	2.330(3)	2.125(2)
C(1A)–O(1A)	1.270(3)	1.259(3)	1.267(4)	1.262(4)
C(1A)–O(2A)	1.234(4)	1.236(3)	1.233(4)	1.230(4)
C(1B)–O(1B)	1.232(4)	1.237(3)	1.227(4)	1.226(4)
C(1B)–O(2B)	1.259(3)	1.261(3)	1.272(4)	1.261(4)
C(1C)–O(1C)	1.257(4)	1.268(3)	1.248(4)	1.258(4)
C(1C)–O(2C)	1.244(4)	1.236(4)	1.248(4)	1.230(4)
O(1A)–M–O(1A)#1	180.0	180.0	180.0	180.0
O(2B)#2–M–O(2B)#5	180.0	180.0	180.0	180.0
O(1C)–M–O(1C)#1	180.0	180.0	180.0	180.0
O(1A)–M–O(2B)#2	90.73(7)	90.66(7)	91.25(9)	90.89(8)
O(1A)–M–O(1C)	96.20(8)	95.58(8)	96.11(9)	96.14(9)
O(2B)–M–O(1C)#5	94.92(8)	94.41(8)	94.52(9)	94.92(9)
O(1A)–C(1A)–O(2A)	125.6(3)	126.0(3)	125.0(3)	125.8(3)
O(1B)–C(1B)–O(2B)	126.6(3)	126.3(3)	126.1(3)	126.5(3)
O(1C)–C(1C)–O(2C)	127.5(3)	127.6(3)	127.7(3)	127.7(3)

Symmetry codes: #1 $-x, -y, -z$; #2 $-x-1, -y, -z$; #3 $-x, -y, -z+1$; #4 $-x-1, -y+1, -z$; #5 $x+1, y, z$; #6 $x-1, y, z$; #7 $-x, -y+1, -z+1$; #8 $x-1, y+1, z$.

the three independent formate groups and the two aqua molecules. From the eight independent available oxygens, O2C does not coordinate at all (but see the H-bonding description below) and O1A makes a single coordination to Ba; the remaining six, however, behave as (short) bridges between cations linking them in a direct $Cat_1-O-Cat_2$ mood, and carboxylates A and B, in turn act as (long) bridges of the $Cat_1-O_1-C_1-O_2-Cat_2$ type. The result is a 3D polymeric structure which basic structural unit has already been found in other compounds of the sort: this is a broad strip running along the crystallographic *b* axis and composed by an internal chain of interlinked Ba coordination polyhedra built up around the two types of symmetry centers disposed along *b*. The M octahedra, in turn, attach externally to this chain to configure the broad strips shown in Fig. 2. A very similar pattern has been observed in the recently reported $SrCu(COOH)_4(H_2O)_2$ [16], to which paper we refer for a detailed description of the motive (thus omitted herein) and in $Sr_2Cu(COOH)_6(H_2O)_4{\cdot}4(H_2O)$ [17] where the only differences arise in the characteristics of the M coordination polyhedra and in the way the strips interact with each other; in both cases there is a covalent linkage leading to sheets in the (001) plane, but while in the Sr_2Cu case the interplane interactions involve just H-bonding contacts, in the present structures this binding is achieved through a bridging formate (A), providing a Ba–O1A–C1A–O2A–Ba′ link directed along the c axis.

Fig. 3 shows a packing view along the crystallographic *b* axis, showing channels which contain the water molecules sites. Analogous ducts exist along the remaining two axis, all of which constitute economic paths to get out from the structure, once detached from the Ba coordination polyhedra.

Table 4
Assignments of the hydrogen bonds in $Ba_2M(CHOO)_6(H_2O)_4$

M	Hydrogen bonds	ν_{OD}, 25°C	ν_{OD}, −180 °C	$O_w\cdots O$ exp.	$O_w\cdots O$, calc.	O–H, calc.	$H\cdots O$, calc.	$<OH\cdots O$, exp.	Σ_O (v.u.)
Co	H1WA···O2C	2441	2430	2.787 (1.48)	2.746	0.972	1.791	162	1.48
	H1WB···O2C	2468	2472	2.815 (0.79)	2.793	0.967	1.841	171	
	H2WB···O2C	2477	2472	2.841 (1.70)	2.793	0.967	1.841	171	
	H2WA···O2A	2587	2577	3.065 (3.52)	2.957	0.955	2.014	169	1.77
Ni	H1WA···O2C	2435	2425	2.791 (1.81)	2.741	0.972	1.786	166	1.52
	H1WB···O2C	2472	2467	2.816 (1.04)	2.787	0.967	1.835	175	
	H2WB···O2C	2472	2467	2.829 (1.49)	2.787	0.967	1.835	169	
	H2WA···O2A	2587	2577	3.047 (2.95)	2.957	0.955	2.014	175	1.75
Cu	H1WA···O2C	2420	2420	2.789 (1.92)	2.735	0.973	1.780	148	1.47
	H1WB···O2C	2456	2441	2.788 (1.10)	2.757	0.971	1.803	174	
	H2WB···O2C	2488	2478	2.880 (2.77)	2.800	0.966	1.849	161	
	H2WA···O2A	2566	2556	3.008 (3.04)	2.917	0.957	1.972	171	1.76
Zn	H1WA···O2C	2441	2425	2.777 (1.31)	2.741	0.972	1.786	162	1.54
	H1WB···O2C	2468	2472	2.808 (0.54)	2.793	0.967	1.841	174	
	H2WB···O2C	2477	2472	2.831 (1.35)	2.793	0.967	1.841	172	
	H2WA···O2A	2592	2577	3.061 (3.39)	2.957	0.955	2.014	174	1.78

ν_{OD}, uncoupled OD stretches at ambient and liquid nitrogen temperatures; intramolecular O–H and intermolecular $H\cdots O$ and $O_w\cdots O$ bond distances; O–H, calculated according to [20], $H\cdots O$ and $O_w\cdots O$, calculated according to [18] (ν_{OD} in cm^{-1}; bond distances in Å; bond angles in °; Σ_O in valence units, calculated according to [21]; in parentheses: deviations from the Mikenda's [18] curve in per cent).

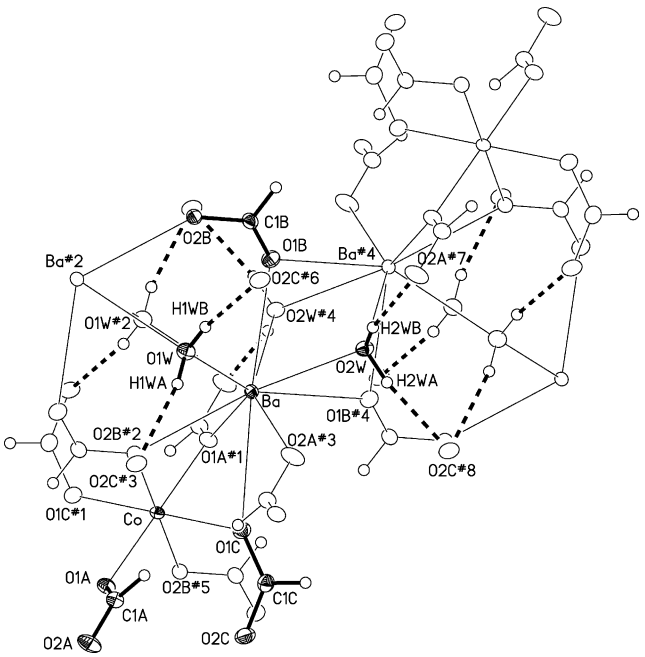

Fig. 1. Ba and M coordination polyhedra (M: Co, representing the whole series) showing the numbering scheme used, and suggesting the way in which the polymer builds up. Full shaded ellipsoids (drawn at a 40% level) correspond to independent atoms; open ones, to atoms generated by symmetry. H-bonds drawn as broken lines. For symmetry codes refer to footnote in Table 3.

3.2. Thermal behavior

Relevant TGA data are presented in Table 5. The good agreement between calculated and experimental values of weight loss indicates that the dehydration process in all cases takes place in one well differentiated stage after which the decomposition process starts.

In spite of the structural similarities in the barium site (the one to which the water molecules are attached) there are some significant differences in the dehydration onset. The process starts quite early in the copper compound, the only one which presents a definite diverse coordination in the M site, followed by the zinc one at intermediate temperatures, and with the remaining two (Co and Ni) not showing significant differences in the way they lose their water molecules, at a definite higher temperature.

This behavior is rather surprising since no direct interaction of the M cations with the water molecules exists, and suggests a much more indirect mechanism of destabilization than previously suspected.

3.3. Hydrogen bonding systems

The strengths of hydrogen bonds in solids result from both the relative hydrogen bond donor strengths and the relative hydrogen bond acceptor capabilities of

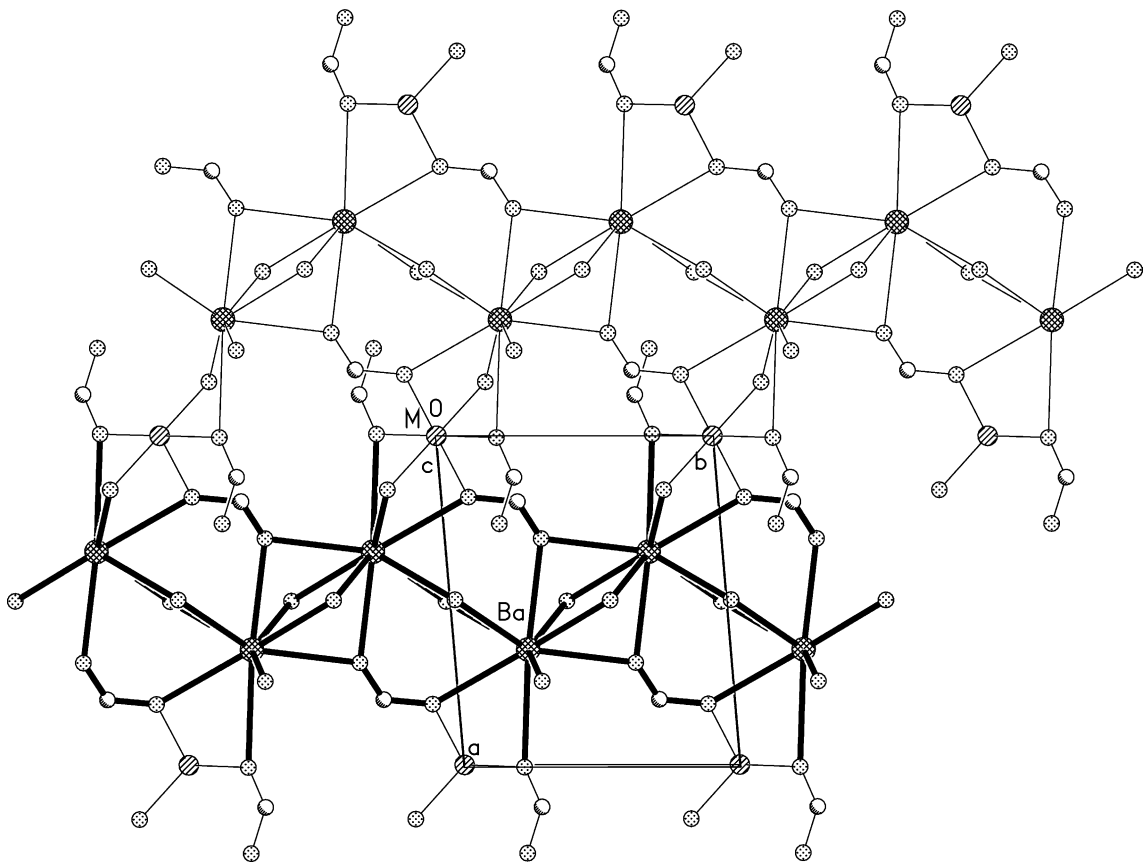

Fig. 2. Packing of the structure viewed down the crystallographic *c* axis. Note a (highlighted) strip running along *b*.

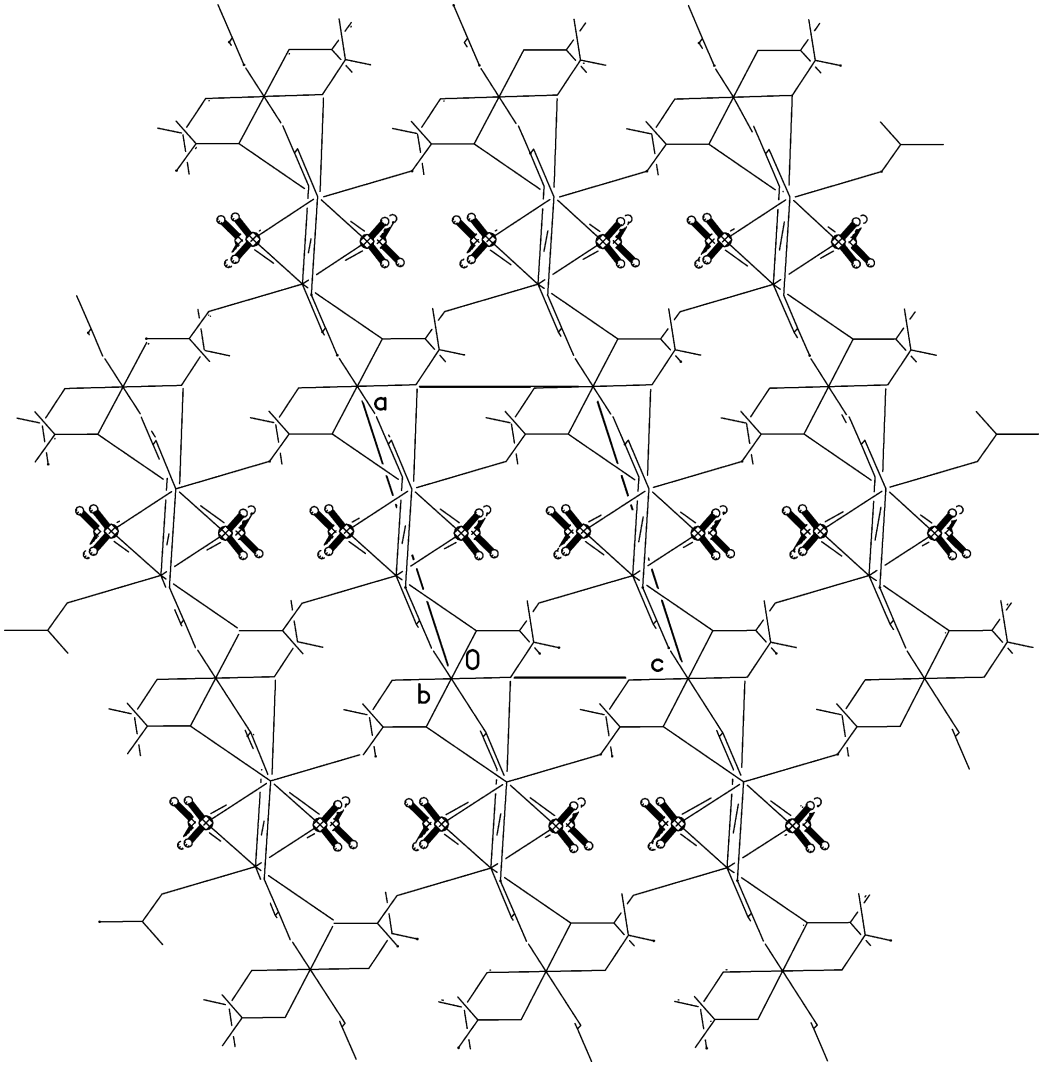

Fig. 3. Packing view along *b*, showing channels occupied by the aqua molecules.

the respective hydrogen bond donor and acceptor groups. These strengths are additionally modified by bonding interactions of the donors and acceptors with other entities of the structure (synergetic effect, co-operative and anti-cooperative (competitive) effects), etc. [8] and references therein.

The existence of two crystallographically different water molecules in the compounds under study, WA and WB, (each type in C_1 site symmetry, i.e. four different OH oscillators) will result in an appearance of four infrared bands corresponding to four uncoupled OD stretches of matrix-isolated HDO molecules (isotopically dilute samples). IR spectra of the double salts in the region of the OH and OD stretching modes are presented in Fig. 4 (see also Table 4).

Fig. 4 shows that the OD bands exhibit red-shifts upon cooling (i.e. $d\nu/dT > 0$), thus indicating the formation of linear hydrogen bonds (i.e. $<OH\cdots O > \ 140°$) in

Table 5
Thermogravimetric data

Compounds	MW	Dehydration onset (°)	Weight loss		Residual	
			Expected for 4(H_2O) (%)	Found (%)	Expected for $BaCO_3$ + MO (%)	Found (%)
$Ba_2Co(HCOO)_6(H_2O)_4$	675.78	145	10.66	10.6	19.83	20.3
$Ba_2Ni(HCOO)_6(H_2O)_4$	675.56	149	10.66	10.9	19.85	21.0
$Ba_2Cu(HCOO)_6(H_2O)_4$	680.39	79	10.58	10.0	19.70	21.7
$Ba_2Zn(HCOO)_6(H_2O)_4$	682.22	92	10.56	10.2	19.65	19.6

agreement with the structural data. The comparatively large Ba–OH_2 bond distances and the ionic character of the respective bonds determine weak metal–water interactions (i.e. weak synergetic effect). Hence, the hydrogen bond strengths will be influenced predominantly by the hydrogen bond acceptor capability of the formate oxygen atoms. As a measure of the proton acceptor strength it might be used the Brown's bond-valence sum of the oxygen atoms—the smaller the bond-valence sum, the higher the proton acceptor strength. Thus, the non-coordinated to the metal ions O2C exhibits high hydrogen bond acceptor capability and as a result it is involved in three hydrogen bonds (Table 4). The monodentately bonded to barium oxygen atom O2A displays lower proton acceptor capability due to the competitive effect and is involved in the weakest hydrogen bond with H2WA. The WA molecules which form the strongest and the weakest hydrogen bonds are strongly asymmetrically hydrogen bonded and their distortion increases in order Cu < Co < Ni ≈ Zn (as a measure of this distortion is used the difference between the higher and the lower wavenumbered ν_{OD}). The WB molecules are

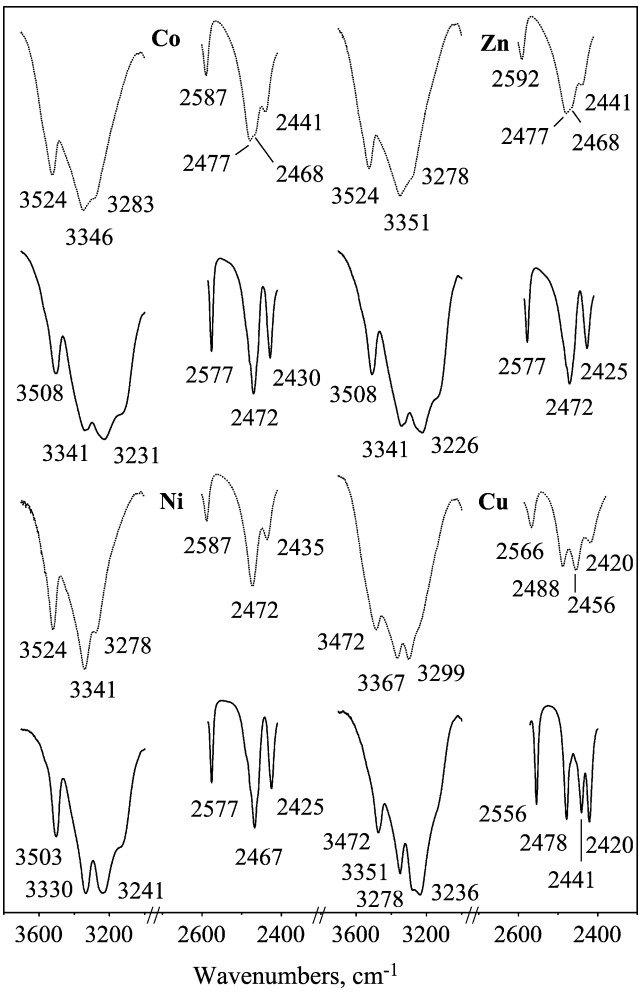

Fig. 4. Infrared spectra of isotopically dilute samples (8–10% D_2O) in the region of uncoupled OD stretching modes (wavenumbers in cm^{-1}; …, ambient temperature; —, liquid nitrogen temperature).

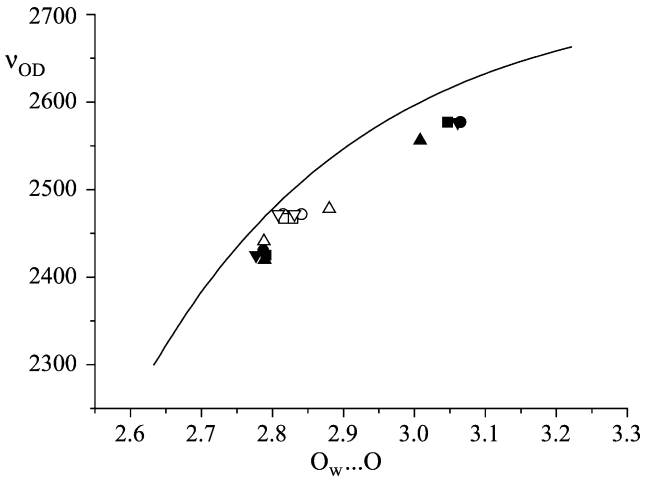

Fig. 5. Correlation of the wavenumbers of uncoupled OD stretching modes with experimental $O_w\cdots O$ bond distances in the double formates (correlation curve reported by Mikenda [18]; full signs, WA; empty signs, WB; △, copper; ○, cobalt; □, nickel; ▽, zinc).

symmetrically hydrogen bonded in the case of the cobalt, nickel and zinc compounds as deduced from the infrared wavenumbers of the respective ν_{OD} (only one band corresponding to the two hydrogen bonds formed by WB are observed in the spectra). The intermolecular $O_w\cdots O$ and $H\cdots O$ bond distances calculated according to the traditional correlation curve of Mikenda [18] are presented in Table 5 (see Fig. 5). Fig. 5 shows that the hydrogen bonds formed by WA are stronger than predicted from the correlation curve as compared to those formed by WB and consequently, as a whole the WA molecules form stronger hydrogen bonds than WB (the deviations from the Mikenda's curve in per cent are calculated as mean values of the respective wavenumbers, see figures in parentheses).

Lutz et al. [19,20] have established linear correlations between the intramolecular bond-valences $s_{OH(D)}$ and $s'_{OH(D)}$ of water molecules in condensed materials and the wavenumbers of the respective uncoupled OD stretching modes of matrix-isolated HDO molecules. According to the authors the correlation curves proposed allow to calculate the intramolecular OH bond lengths on the basis of the infrared and Raman spectroscopic studies and the data thus obtained are mostly more accurate than even those determined from neutron diffraction studies (for the OH bond lengths see Table 4).

4. Conclusions

The crystal structures herein reported confirm the tendency of mixed formates to produce densely packed polymers. As in other related compounds the structural motif consists of broad strips containing both types of polyhedra, here interlinked through covalent bonds to produce a tightly woven 3D network. The present description of the M = Co, Ni, Cu, Zn series, which corrects

a previous structural report on the copper moiety in Ref. [2], allows a straightforward interpretation of the similarity in H-bond strengths, but on the other hand, leaves some unanswered questions regarding differences in the dehydration temperature onset along the series.

The analysis of the IR spectra in the region of the uncoupled OD stretches (2400–2600 cm^{-1}) reveals: (i) the weak $Ba-OH_2$ interactions (large bond distances and ionic character of the respective bonds) are a reason for the formation of weak hydrogen bonds in the double formates. The fact that the water molecules are not bonded to the metal ions of 3d series explains the formation of hydrogen bonds of similar strength. (ii) The hydrogen bond strengths are influenced predominantly by the different hydrogen acceptor strengths of the formate oxygen atoms. Thus, the non-coordinated to the metal ions O2C act as stronger acceptor than monodentately bonded to barium O2A (competitive effect) in correlation with their bond-valence sums. (iii) All hydrogen bonds formed are stronger than predicted from the correlation curve of Mikenda, thus indicating that the formate ions as a whole are comparatively strong hydrogen bond acceptors.

References

[1] D. Stoilova, V. Koleva, Cryst. Res. Technol. 32 (1997) 865.
[2] R.V.G. Sundara Rao, K. Sundaramma, G. Sivasankara Rao, Z. Kristallogr. 110 (1958) 231.
[3] D. Stoilova, V. Koleva, J. Mol. Struct. 404 (1997) 291.
[4] D. Stoilova, S. Peter, H.D. Lutz, Z. Anorg. Allg. Chem. 620 (1994) 1793.
[5] D. Stoilova, H.D. Lutz, J. Mol. Struct. 450 (1998) 101.
[6] D. Stoilova, V. Koleva, J. Mol. Struct. 560 (2001) 15.
[7] D. Stoilova, M. Wildner, V. Koleva, J. Mol. Struct. 643 (2002) 37.
[8] H.D. Lutz, J. Mol. Struct. 646 (2003) 227.
[9] L.S. Itkina, K.A. Nadzharyan, I.I. Lepeshkov, Zh. Neorg. Khim. 24 (1979) 2244.
[10] Bruker-AXS, SMART V5.625, Data Collection Software, Bruker Analytical X-ray Instruments Inc., Madison, Wisconsin, USA, 2001.
[11] Bruker-AXS, SAINT V6.28A, Data Reduction Software, Bruker Analytical X-ray Instruments Inc., Madison, Wisconsin, USA, 2001.
[12] Bruker-AXS, SADABS, Area Detector Absorption Correction Program, Bruker Analytical X-ray Instruments Inc., Madison, Wisconsin, USA, 2001.
[13] G.M. Sheldrick, SHELXS97 and SHELXL97: Programs for Structure Resolution and Refinement, University of Göttingen, Germany, 1997.
[14] Bruker-AXS, SHELXTL-NT/2000, Version 6.1, Bruker Analytical X-ray Instruments Inc., Madison, Wisconsin, USA, 2000.
[15] F.H. Allen, O. Kennard, Chem Des Autom News 8 (1993) 131.
[16] R.F. Baggio, P.K. de Perazzo, G. Polla, Acta Crystallogr. C41 (1985) 194.
[17] A. Goeta, R. Baggio, D. Stoilova, Vib. Spectrosc. 34 (2004) 293.
[18] W. Mikenda, J. Mol. Struct. 147 (1986) 1.
[19] H.D. Lutz, C. Jung, M. Trömel, J. Lösel, J. Mol. Struct. 351 (1995) 205.
[20] H.D. Lutz, C. Jung, J. Mol. Struct. 404 (1997) 63.
[21] N.E. Brese, M. O'keeffe, Acta Crystallogr. B47 (1991) 192.